Bull. Inst. Chem. Res., Kyoto Univ., Vol. 70 No. 5-6, 1993

High Resolution Electron Spectromicroscope (HRESM), Applications

Sakumi MORIGUCHI*, Akitaka HOSHINO*, Syugo HASHIMOTO*, Koji KUBONO*, Kazuhiro NAGAI*, Noriko ASAKA*, Tetsuya OGAWA*, Hiroki KURATA*, Seiji ISODA* and Takashi KOBAYASHI*

Received December 16, 1992

High resolution images of several inorganic and organic materials were taken to elucidate the ability of a new 1000 kV high resolution electron spectromicroscope (HRESM) installed in Kyoto University. These results have proved that the resolving power of the microscope is better than 0.12 nm.

KEY WORDS: High voltage/ High resolution/ Spectromicroscope/ Imaging plate/ Gold/ Gallium arsenide/ Phthalocyanines/ Fullerens

1. INTRODUCTION

After the success to image the crystal lattice of phthalocyanine,[1] there have been many efforts to obtain higher resolution with transmission electron microscope. In particular, Uyeda et al. have realized the atomic image in a crystal of copper perchloro-phthalocyanine ($Cl_{16}CuPc$) by "many-beams synthesis" method with the 500 kV high resolution electron microscope at Kyoto University.[2] This many-beams synthesis method has widely spread over all fields of electron microscopic studies. Though in these times another type of high resolution microscopy technique, i.e., scanning tunneling microscopy, was developed successfully under a different concept,[3] this method is unfortunately applicable only to the observation of surface structures. Transmission electron microscopy is, therefore, still important method to investigate the crystal structure of materials. We have designed a new 1000 kV transmission electron microscope, which will realize a high resolution of about 0.12 nm as the point-to-point resolution.[4] This new 1000 kV electron microscope can analyze the energy loss of incident electrons passed through specimens, and accordingly this electron microscope was named "High Resolution Electron Spectro-Microscope (HRESM)".[5]

In this paper, we report several high resolution images obtained with the HRESM and its practical performance for actual specimens.

2. EXPERIMENTAL

Since sufficiently thin specimens is required in order to obtain a high resolution

* 森口作美, 星野聡孝, 橋本修吾, 久保埜公二, 永井一弘, 安積典子, 小川哲也, 倉田博基, 磯田正二, 小林隆史 : Division of States and Structures II, Institute for Chemical Research, Kyoto University, Uji, Kyoto-611, Japan

image,[6] very thin specimens were prepared by vacuum deposition or crushing methods, and supported on thin carbon films fixed beforehand on perforated-microgrids on copper meshes. Observation with HRESM was performed at an accelerating voltage of 1000 kV or 800 kV, and in the case of organic materials a minimum dose system was used to deduce the undesirable electron radiation damage of specimens. The detailed experimental procedures will be described for the respective specimens in the following sections.

3. RESULTS AND DISCUSSION

3-1. Phase contrast transfer function

It is known that the phase transfer function of an objective lens for thin specimen is principally determined by the spherical aberration coefficient Cs, the defocus value Δz and the wave length of electron λ. However, the phase transfer function is practically modified by other factors in the form of envelope functions due to the energy spread of incident electron, instability of magnetic lenses, the electron beam divergence on the specimen surface and the atomic scattering factor of the constituent atoms of the specimen, etc. Therefore, the performance of HRESM was firstly confirmed by taking high resolution image of a thin amorphous germanium film prepared by vacuum deposition, whose thickness was determined to be about 2 nm by measuring the intensity of energy loss due to multiple plasmon excitation in the film.[7] The Fourier transform of the image of the amorphous film represents the practical phase transfer function, so long as the specimen is thin enough to be assumed a weak phase object. Fig. 1-a shows an example of diffractogram, i.e., optical Fourier transform of the high resolution image of the amorphous germanium film taken at the Scherzer focus, 44 nm under focus at 1000 kV. Fig. 1-b is the corresponding phase transfer function calculated from the known Cs, Δz and λ. In addition to these factors, the following envelope functions are taken into account; the effects of the atomic scattering factor of germanium, the beam divergence ($\beta_i = 1$ mrad) and the apparent total energy spread of electron ($\Delta E/E = 3 \times 10^{-6}$, including all contributions from the Boersch effect,[8] the high voltage and magnetic lens instabilities). Fig. 1-a represents that the effective phase contrast transfer function has finite values up to the spatial frequency of $(0.12\ \text{nm})^{-1}$, even though its values are attenuated in the higher spatial frequency region. The Bragg spots in the diffractogram shows a spacing of gold (222) corresponding to 0.118 nm. This clearly proved that the potential performance of the HRESM reaches to the expected level in the practical situations.

3-2. Inorganic Materials

3-2-1. Multiple-twinning in gold crystal

Twinning is the most common crystal-growth defect, and many twinned crystals have been imaged by high-resolution electron microscopy. Fig. 2 shows an example of such twinning in a very fine gold particle evaporated directly onto an amorphous carbon film; the simplest possible twin in face-centered-cubic crystals.[9] This twining is known to be the $\Sigma 3(111)$ grain boundary and the twinning has been observed as pentagonal multiple-twins as indicated by the arrows in the figure, which were introduced during the growth of the gold particle on the amorphous carbon film. Until recently, the available microscope re-

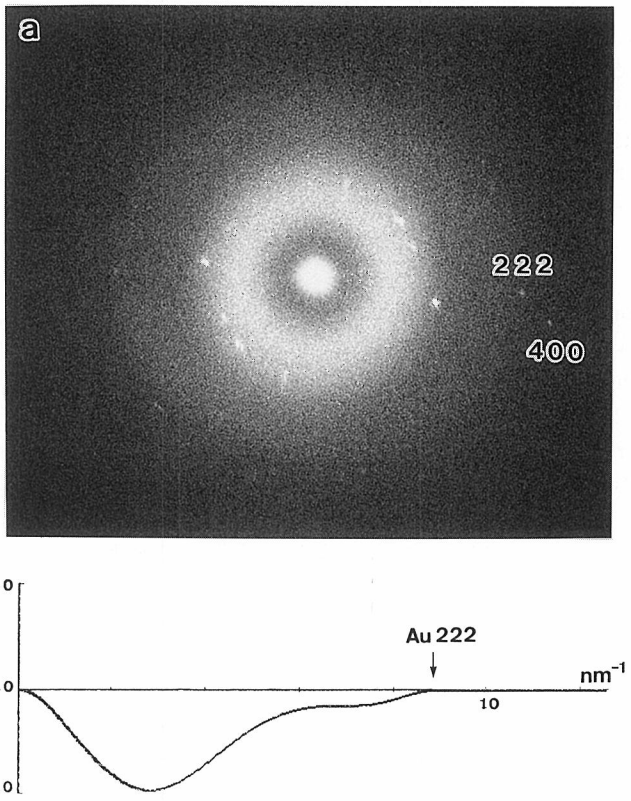

Fig. 1 (a) Optical diffractogram of a high resolution image of ultra thin amorphous germanium film taken at the Scherzer focus of 1000 kV. The first transfer band of the phase transfer function expands up to the spatial frequency of the 222 reflection of gold crystal, though the intensity decreases at higher region.
(b) Simulated phase transfer function considering the spherical aberration coefficient, the defocus, the wave length and also some envelope functions due to the energy spread and the beam divergence.

solution prevented such high resolution structure imaging of multiple-twin from being obtained and only the appearance of a boundary image was reported. Such an image is not generally an accurate guide to investigate the lattice relaxation (displacements of atoms) at the twin interface, which is one of the important subjects to understand the mechanical properties of metallic materials. However, the structure image taken with the HRESM made it possible to measure the boundary displacements.

3-2-2. GaAs

An atomic structure image has not been obtained from any elemental or binary semiconductor using any microscope so far, as evident from their resolution.[10] However, the HRESM has proved to have the potential to resolve atom-atom distances in such materials, eg. gallium-arsenide GaAs. The specimen of GaAs was prepared by the crushing method

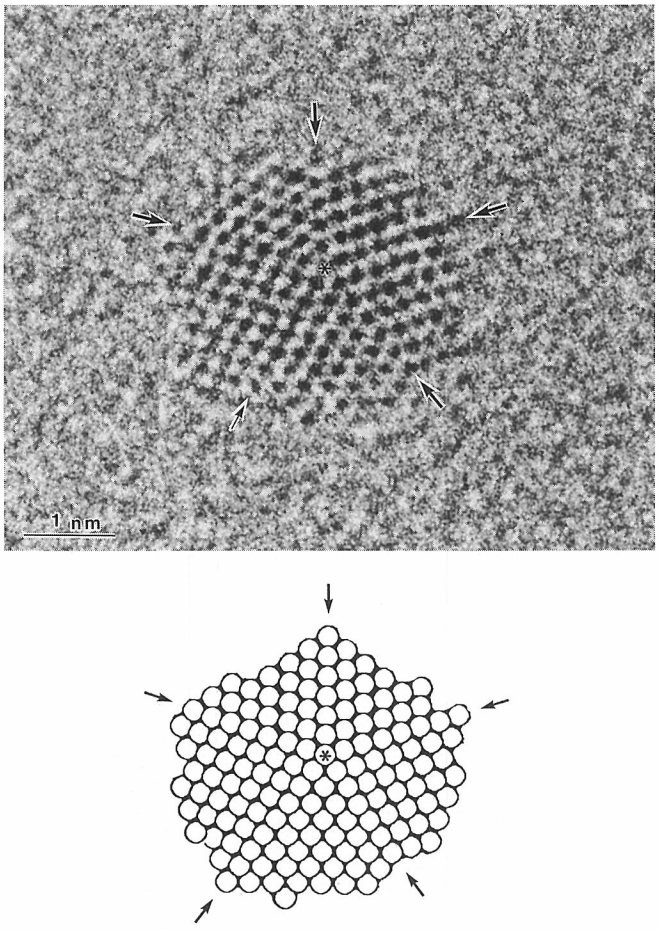

Fig. 2 Multi-twin structure observed in a fine gold particle. The drawing represents the Wulff-faceted decahedral symmetric particle viewed along the [110], which possesses an five-fold symmetry.

and was fixed on a thin amorphous carbon film. The high resolution image was taken near the crystallite edge at 1000 kV by adjusting the crystal orientation with a goniometer stage (tilting angle $\pm$ 40°). Fig. 3-a shows an example of the high resolution image as the projection along the [110] direction. Fig. 3-b is the optical transform of the image in Fig. 3-a, where the reflection spots up to the (442) spacing of 0.094 nm are observed. The Ga and As spaced 0.14 nm along the c-axis have the similar atomic scattering factor so that it is hard to distinguish between Ga and As in the image. Fig. 4 shows the simulated images of GaAs at energy fluctuation of $\Delta E/E = 1 \times 10^{-6}$ (b) and $\Delta E/E = 5 \times 10^{-6}$ (c) together with the projected potential map (a). In the case of $\Delta E/E = 1 \times 10^{-6}$, Ga and As can be observed as separated atomic images, otherwise both atomic images are barely resolved owing to the image deterioration caused by chromatic aberration as shown in Fig. 4-c. The actual image in Fig. 3-a corresponds to the case of $\Delta E/E = 3 \times 10^{-6}$.

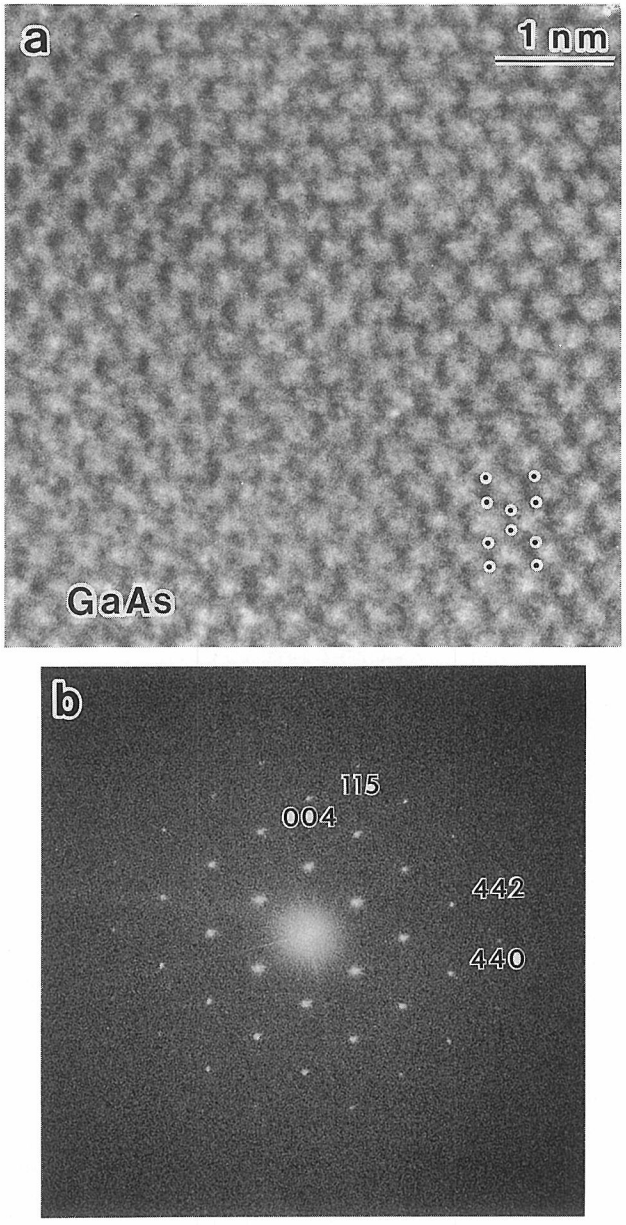

Fig. 3 (a) High resolution image of GaAs as the projection along the [110].
(b) Optical diffractogram of (a) showing up to the 442 reflection.

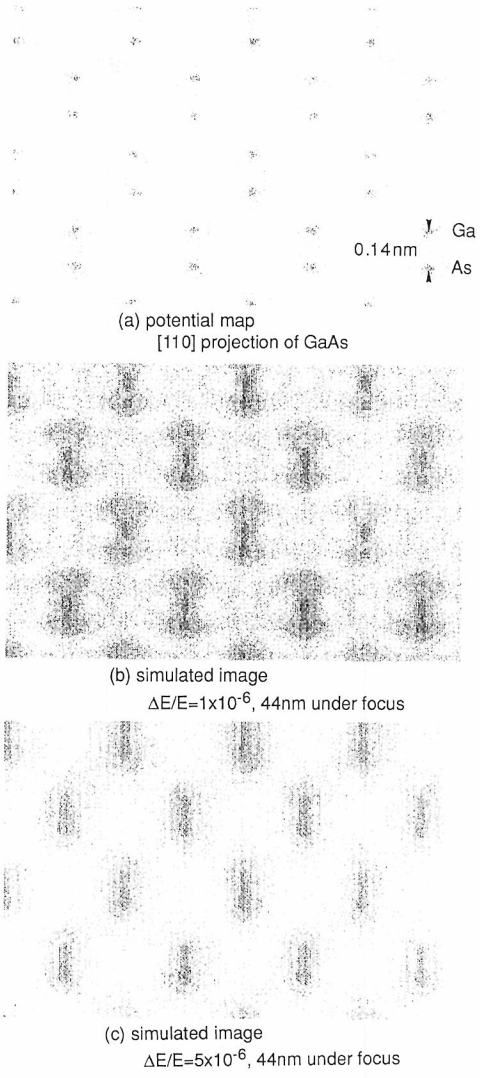

Fig. 4 Potential map of GaAs (a). Simulated images as the projections along the [110] at $\Delta E/E = 1 \times 10^{-6}$ (b) and $\Delta E/E = 5 \times 10^{-6}$ (c) for 1000 keV electrons.

3-2-3. Graphite

Graphite is a good sample for testing the resolving power for carbon-carbon distance in an organic material, because it has a benzene-like structure as a part. The graphite specimen was peeled off by ultrasonic power and then fixed on a thin carbon films for electron microscopic observation. Fig. 5-a is a high resolution image taken at 1000 kV, which corresponds to the c-axis projection of the crystal. Fig. 5-b shows the optical transform of the image in Fig. 5-a. The images of carbon atoms are clearly observed. In this case, however, the image contrast of the projected column (A-column indicated by "A" in Fig. 6),

which contains twice the carbon atoms than the B-column shown by "B" in Fig. 6, is highly enhanced. It is a great difference with the results obtained for a thick specimen with a conventional electron microscope. In the case of the thick specimen, only the (100) and (110) lattice fringes are often observed as an incoherent superposition so that the carbon atoms are imaged with equal intensity at every atom position. However, the carbon columns A and B should be imaged really with different contrasts as shown in Fig. 6, when the specimen is thin enough and the resolving power of the electron microscope is high enough. As demonstrated in the simulations in Fig. 6-b and c, a reasonable accordance with the real images is observed when one assumes $\Delta E/E = 4 \times 10^{-6}$.

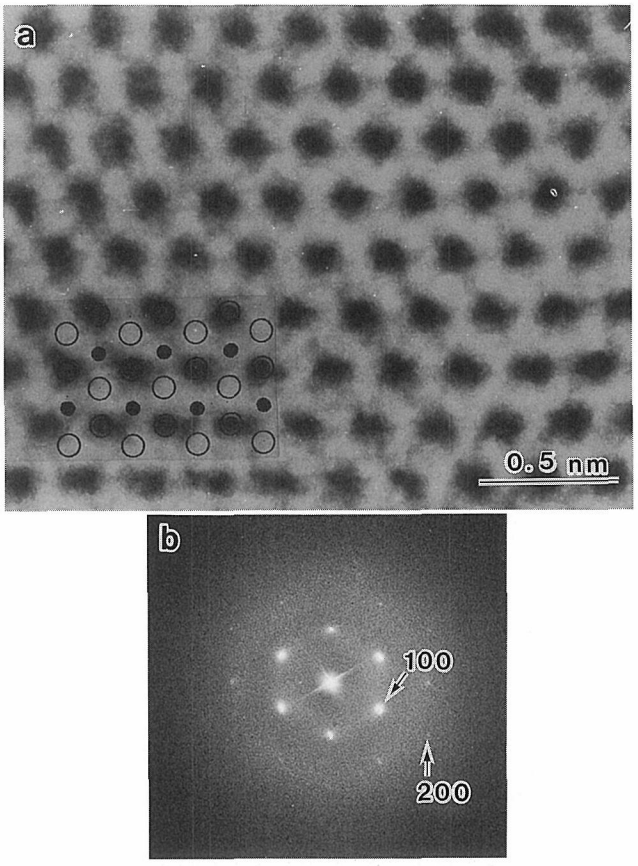

Fig. 5 (a) High resolution structure image of graphite projected along the c-axis.
(b) Optical diffractogram of (a).

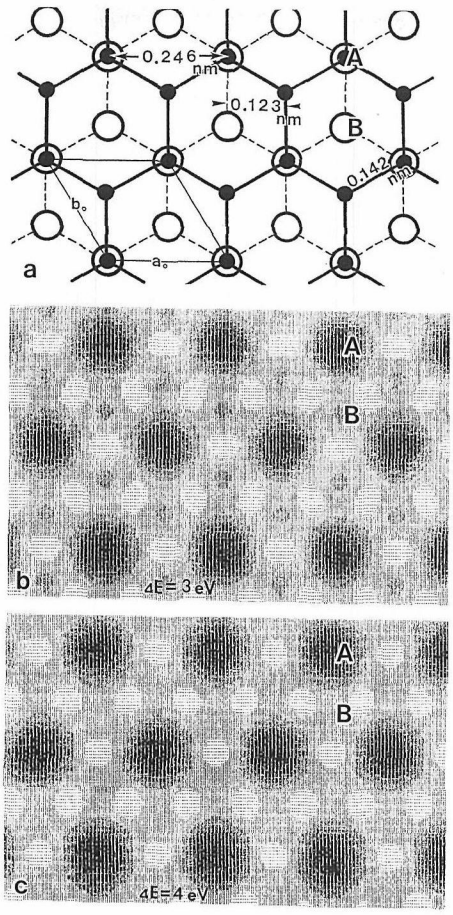

Fig. 6 Atomic arrangement of graphite in the projection along the c-axis (a). Simulated images at $\Delta E/E = 3 \times 10^{-6}$ (b) and at $\Delta E/E = 4 \times 10^{-6}$ (c).

3-3. Organic Materials

For organic materials, high resolution imaging was carried out with the aid of a minimum dose system.[11] The minimum dose system was modified a little so as to make an operation easier in the HRESM.

3-3-1. GeOPc

Poly-germanium-oxy-phthalocyanine $(GeOPc)_n$ is known to crystallized epitaxially on an alkali-halides single crystal surface by vacuum deposition.[12] Fig. 7-a shows a high resolution image observed along the c-axis of the tetragonal crystal (a = 1.372 nm) of GeOPc with the HRESM at 800 kV. In the diffractogram obtained from the image, one can observe the reflections up to the eleventh reflection of the spacing of 0.124 nm. This means that the stability of the minimum dose system in the HRESM is sufficiently high. Fig. 7-b shows a simulated image assuming the staggered stacking structure,[12] together with its crystal structure. The simulated image accords well with the high resolution image,

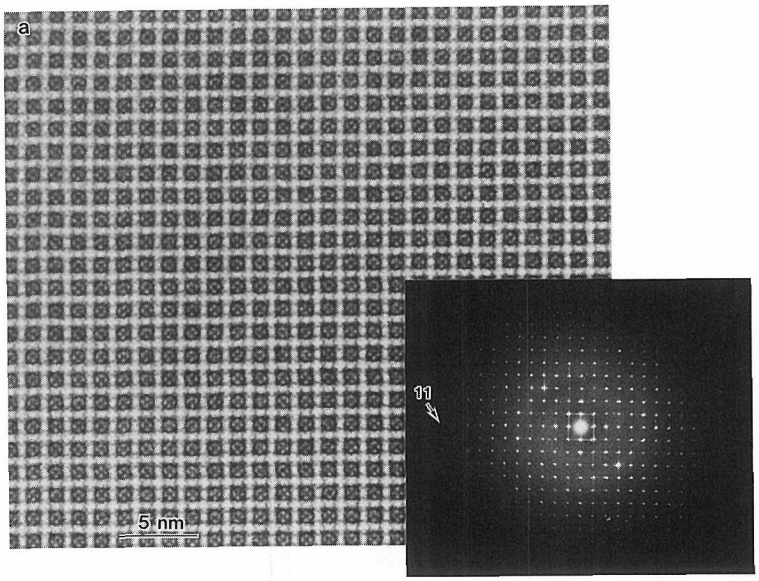

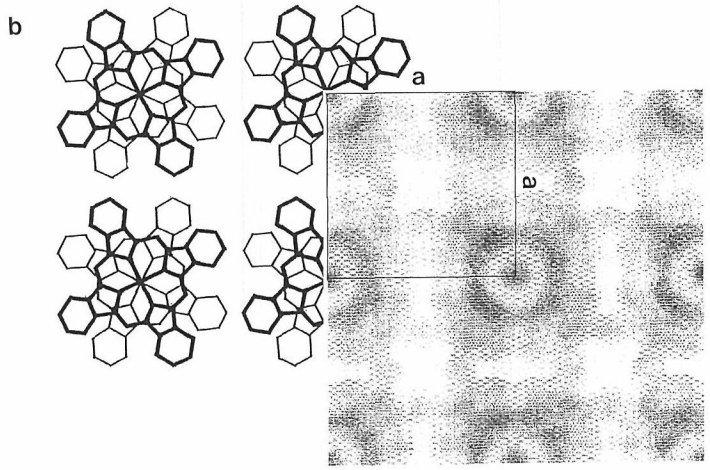

Fig. 7 (a) High resolution image of GeOPc crystallized on the (001) of KCl, where the incident direction of electron is along the c-axis. In the optical diffractogram, the eleventh reflection is observed.
(b) Simulated image from the staggered stacking model, which reproduces well the high resolution image.

which suggests that the staggered structure is a plausible structure model of GeOPc vacuum deposited, though the other eclipsed stacking structure has been proposed for the crystal by X-ray analysis.[13)]

3-3-2. ClTPPFe

In the case of GeOPc the molecules are imaged as isolated molecular columns from

each other in the c-axis projection. However, one could expect the superimposed images of adjacent molecular columns in the c-axis projection of chloro-tetraphenylporphinate-Fe (ClTPPFe), because the material has body-centered-tetragonal structure with the a-axis dimension of 1.353 nm. The ClTPPFe was deposited in vacuum on KCl (001) surface with the thickness of 5 nm. An example is shown in Fig. 8-a, where the black part with a pin-wheel shape corresponds to the densely packed atoms in the projected images. From the known crystal structure of the ClTPPFe,[14] the expected image was simulated for 800 keV electrons, where the overlapped regions and the empty channels are observed to form the characteristic dark pinwheels and the white crosses, respectively (Fig. 8-b). The observed

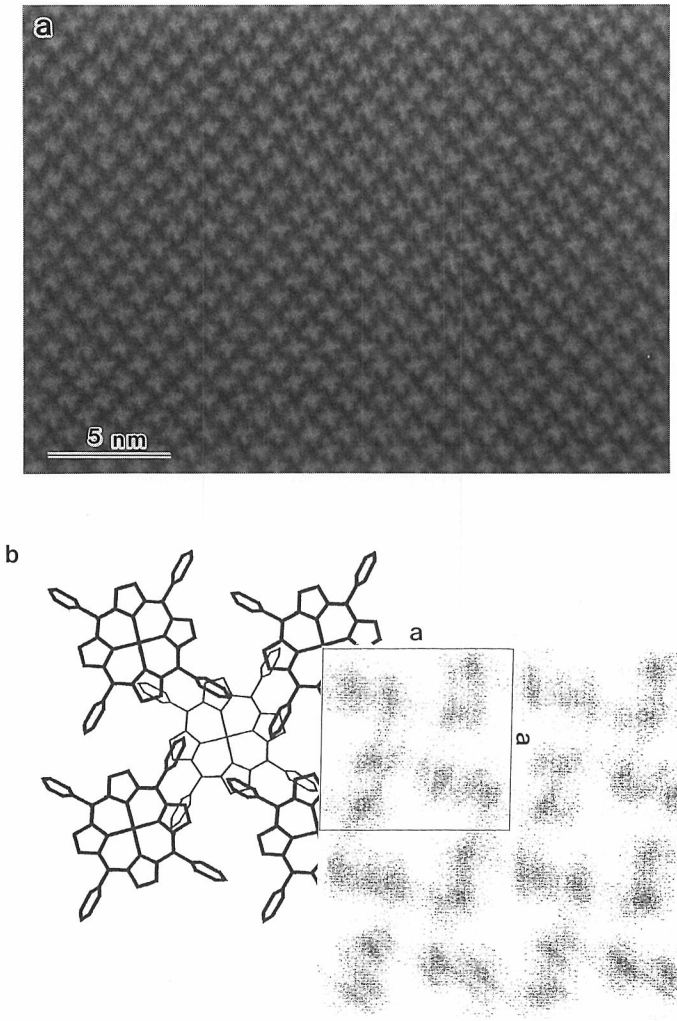

Fig. 8 (a) High resolution image of ClTPPFe crystallized on the (001) of KCl, where the incident beam direction is along the c-axis.
(b) Simulated image from the known tetragonal structure.

images agree well with the simulated one.

The interface of double layer of ClTPPFe and GeOPc was observed with the HRESM as a plan-view projection, and a strange registration mode at the interface was revealed.[15,16)]

3-3-3. AgPc

When silver-phthalocyanine (AgPc) commercially supplied was deposited on a substrate in vacuum, it formed a tetragonal crystal as shown in Fig. 9. However, the silver is completely lost in the deposited film, which was proved by electron energy loss spectrometry and energy dispersive X-ray analysis. Though these analysis of the deposited film showed that the deposited film did not contain any heavy elements, the structure is quite different from the metal-free phthalocyanine. The high resolution image of the film with the HRESM at 800 kV shows a tetragonal arrangement of the molecules on KCl (001) surface as shown in Fig. 9. The molecular images exhibit just the similar contrast as in the tetragonal arrangement of GeOPc. On the other hand, an orthorhombic structure is found on KBr (001) surface, which can also be observed sporadically on KCl as indicated by the arrows in Fig. 9. The tetragonal structure may change into the orthorhombic one by introducing the stacking faults in every two layers.

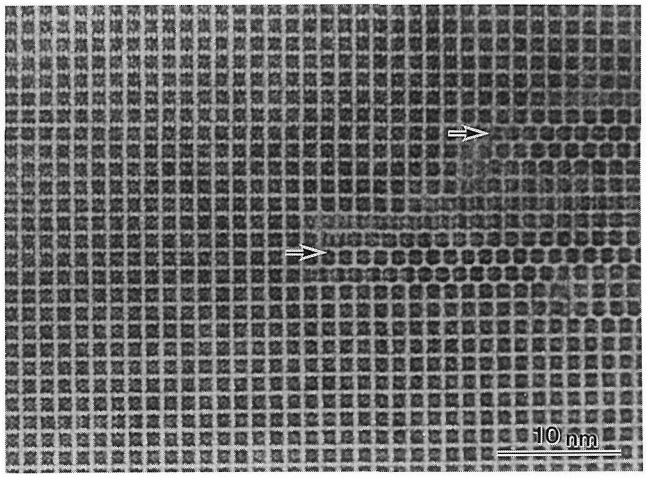

Fig. 9 High resolution image of a thin crystal obtained from vacuum-deposition of AgPc on KCl, which shows a tetragonal arrangement as the case of GeOPc. However, orthorhombic arrangement of molecules are sporadically found as a result of stacking fault.

3-3-4. $Cl_{16}CuPc$

The high resolution images of copper perchloro-phthalocyanine ($Cl_{16}CuPc$) were obtained with the old 500 kV high resolution electron microscope.[2)] It seems worthwhile to compare that with the image taken with the new HRESM. The monoclinic crystal of the $Cl_{16}CuPc$ was grown on KCl through vacuum-deposition and the high resolution image

was taken with the HRESM at 1000 kV as the c-axis projection as shown in Fig. 10-a with its optical diffractogram in Fig. 10-b. The experimental set-up is shown schematically in Fig. 11. The images of a quarter of the molecule are simulated as in Fig. 12 for the former 500 kV (a) and the new 1000 kV HRESM (b). The great difference between the images obtained with the 500 kV and the 1000 kV electron microscopes is the sharpness of the chlorine atoms and the sharpness of the pyrrole rings in the latter images as indicated by the arrows in Fig. 12-c. The carbon and nitrogen atoms are not discriminated even in the 1000 kV because of the wider effective energy spread of electron beam and radiation damage of the specimen. The $Cl_{16}CuPc$ is still damaged during photographing the image, even though the specimen is relatively strong for electron bombardment. Under the irradiation of 1000 keV electrons, the crystal structure of graphite is also destroyed due to the knock-on process; especially serious effect for light elements.

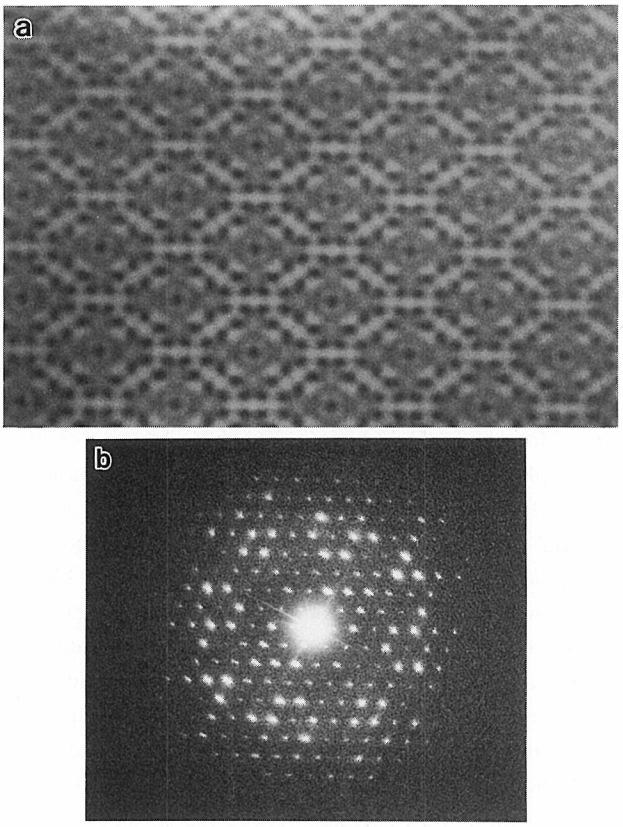

Fig. 10 (a) High resolution image of $Cl_{16}CuPc$ projected along its c-axis.
(b) Optical diffractogram of the image.

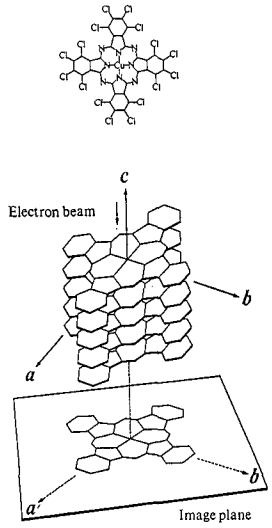

Fig. 11 Geometrical relation between $Cl_{16}CuPc$ molecular column and the electron beam.

3-3-5. C60

Since the fullerenes, C60, are known to cocrystallize with solvent molecules,[17] electron microscopy is expected to give valuable information on pure structure of C60 produced by vacuum-deposition. The C60 was evaporated on KCl, NaCl and KBr (001) surfaces following the usual vacuum-deposition procedure. The evaporated C60 molecules condensed into amorphous phase at the substrate temperature of 20°C, but they formed crystalline state at a higher temperature, for example, above 100°C. The crystal orientations were slightly different from place to place, as expected from the facts that the molecular shape is spherical and its size is larger than the repeat-distance of the (001) substrate surface. The thicker sample gave a hexagonal electron diffraction pattern, which corresponds to the hexagonal[18] or the face-centered-cubic[19] structure. With the HRESM at 1000 kV, very thin crystalline part was imaged as shown in Fig. 13-a, where the C60 molecules, which are imaged as rings, arrange in an orthorhombic structure (shown by the rectangle in the figure). The other orthorhombic structure has been reported for solution including crystal,[20] but the present structure is different in the a- and b-axes dimensions from that. The present orthorhombic structure may come from a stronger interaction between the C60 molecule and the substrate with the four-fold symmetry, which may be observed only in the mono- or double-layers of C60. In the optical diffractogram in Fig. 13-b, strong streaks are observed along the [110] direction. This streaking is caused by the stacking fault indicated by the arrows in Fig. 13-a. On the other hand, the thicker crystalline part gave a hexagonal arrangement of C60 molecules in high resolution image.

The ring image of the C60 comes from the outer part of the molecule, where the atoms are packed densely and give higher contrast in two-dimensional projection as shown in Fig. 14-a, disregarding its rotational motion. Fig. 14-b shows a model of the stacking fault in

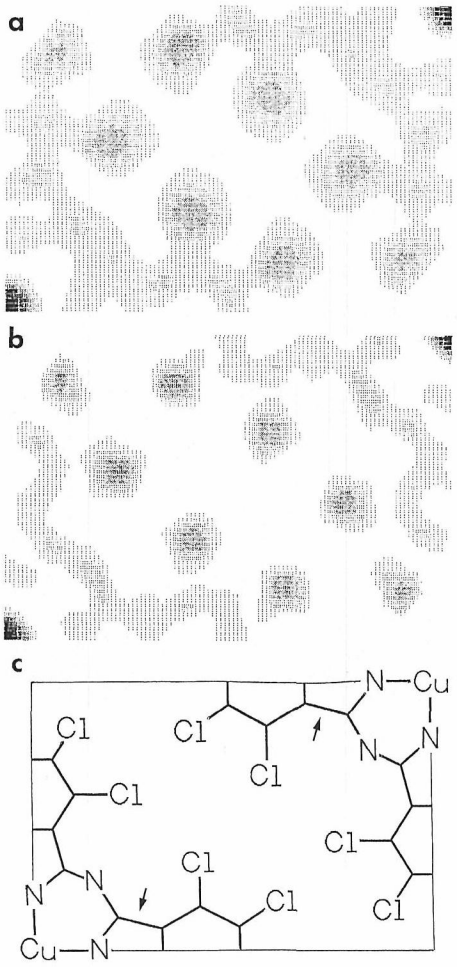

Fig. 12 (a) Simulated image for 500 kV high resolution electron microscope in a quarter of the molecule as shown in (c).
(b) Simulated image for the HRESM.

Fig. 13-a, where the faults happen twice in both sides of the molecular array shown by the dark circles.

During the observation of the thin C60 film, a strange image was observed as shown in Fig. 15, where the molecules indicated by the dots arrange in the orthorhombic unit, but the molecules indicated by the asterisks seem to overgrown on a bridge site of the orthorhombic array as shown schematically in Fig. 15. It suggests that the C60 crystal starts to grow up in a hexagonal-like manner from such a part.

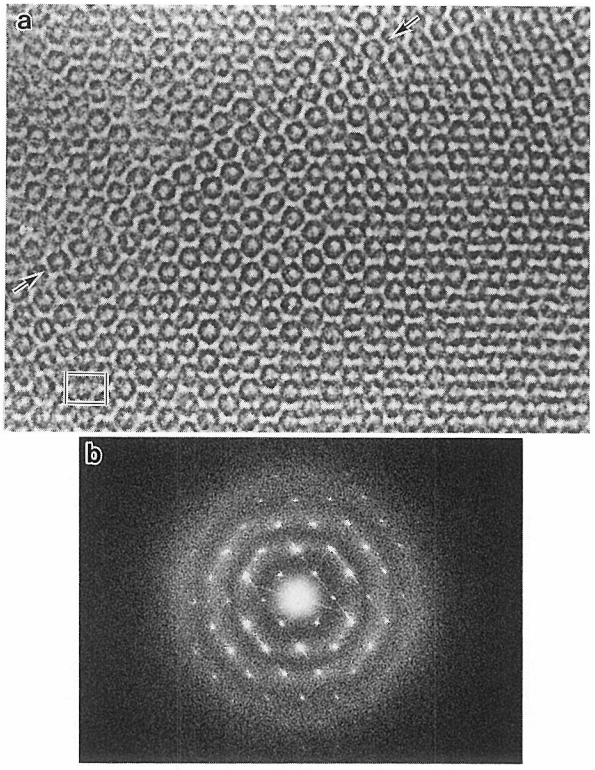

Fig. 13 (a) High resolution image of C60, which shows a orthorhombic structure in a very thin region.
(b) Optical transform of the image, where orthorhombic structure and some stacking faults along the [110] are clearly demonstrated.

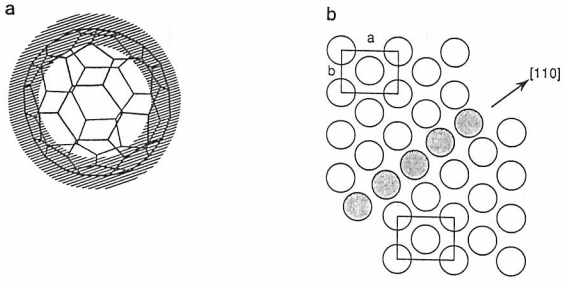

Fig. 14 (a) Expected image for the C60.
(b) Model for the stacking fault along the [110] direction.

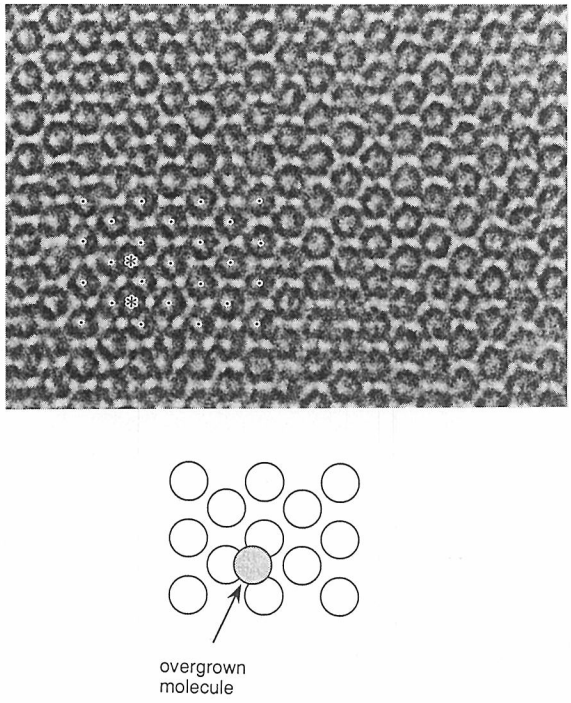

Fig. 15 The molecules (*) are overgrown on the orthorhombic structure shown by the dots.

3-4. Imaging plate

3-4-1. Quantitative analysis of image

The imaging plate (IP) is known as a recording material for electron detection with high sensitivity, good linear response and wide dynamic range.[21] It is particularly useful in quantitative analysis of the electron micrograph. Fig. 16 shows an example of such quantitative image analysis, where the GeOPc molecules near the crystal edge are imaged on IP as described in section 3-3-1. The intensities of the GeOPc image were measured at each image point numbered in the figure, from which the electron densities at the points were measured as in Fig. 16-b. Subtracting the average image intensities at the amorphous carbon, the molecular images at 1 and 2 have been estimated to be about 1/3 of the intensity of the inner part images at 4,5,6,7,8,9 and 10. The image intensity at 3 is the intermediate value between those at 1 or 2 and at the inner parts. This fact means that the crystal grows stepwise at the edge, so that the image intensity changes stepwise with integral multiple of the fundamental crystal unit or the monolayer of the molecules.

3-4-2. Direct structure analysis

The characteristic points of IP are the followings; (1) high sensitivity, (2) linear response and (3) wide dynamic range in electron detection. These characteristics are favorable for measuring electron diffraction intensities. Till now the intensity measurement has been done by using photographic films which are not good detector for such quantitative

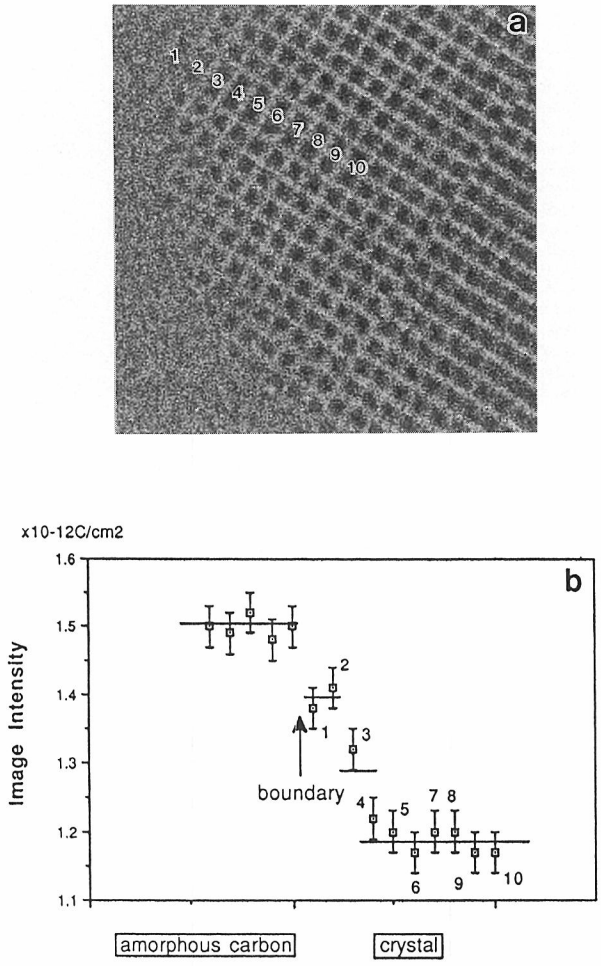

Fig. 16 (a) High resolution image of GeOPc crystal recorded on IP. The intensities of the numbered molecular columns are measured.
(b) Image intensity as a function of the numbers of molecular columns from the crystal edge.

purpose, especially when one aims to analyze a structure of specimen by direct structure analysis. Since some pioneer works on electron crystallography has been started recently using conventional photographic films,[22] the appearance of a good detector was awaited. The present IP system has made it possible to analyze the crystal structure by the following scheme:[23] (i) Electron diffraction pattern is recorded on IP for a correctly oriented crystal, (ii) Intensities of diffraction spots are digitized with a IP-reader, (iii) Applying a direct phasing program for the intensities obtained, the Fourier map is synthesized, (iv) Additional refinements of structure are done. This method is widely applicable when combined with the phase determination from the Fourier transform of high resolution images, and will become the trend of structure analysis especially for organic crystal structure determination

and for many cases where we can obtain only very small crystals.

Figs. 17 and 18 show a test example of structure determination using a thin graphite. Fig. 17 shows the diffraction pattern recorded on IP at 800 kV from very small graphite crystal, and Fig. 18 shows a Fourier synthesis from the intensities of the diffraction spots after applying a direct phasing program. The Fourier map correctly represents separately the A- and B-columns described in Fig. 6 as expected. The diffraction pattern does not affected by the phase transfer function, and therefore more reliable result can be expected for the crystal structure analysis.

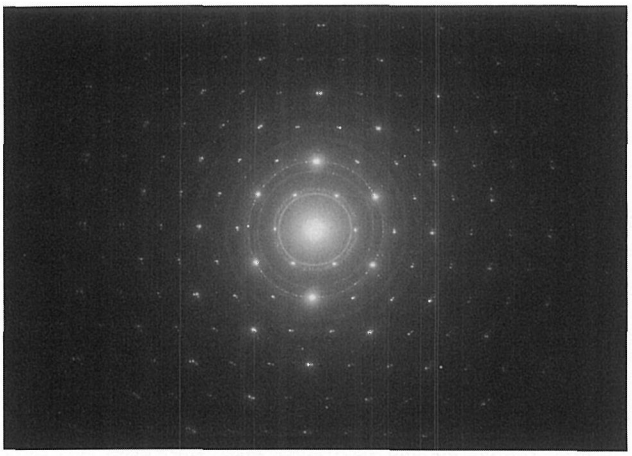

Fig. 17 Electron diffraction pattern of thin graphite crystal recorded on IP as the c-axis projection.

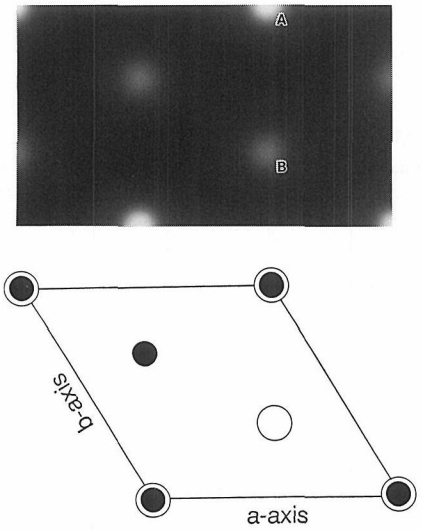

Fig. 18 Fourier synthesis of diffraction of graphite through a direct phasing program.

4. CONCLUSION

The HRESM in Kyoto University having 0.12 nm point-to-point resolution and the new recording system have been proved to be very unique and powerful for structure investigation of many materials. They will give us new information on structure of materials in finer scale.

The most important point in modern electron microscopy is the stability of total microscope system. The total effective energy spread of electrons is about $\Delta E/E = 3 - 4 \times 10^{-6}$ in all cases, which seems to be a very low value compared with other 1000 kV electron microscopes, owing to the twin-tank system in HRESM. Such high stability in the total electron microscope system promises the achievement of high resolution imaging and also high performance of electron spectroscopy, which will be published in near future.

Acknowledgements

The authors wish to thank Prof. Emer. N. Uyeda, Kyoto University, for his effort to introduce the HRESM at the institute. This work has been supported by a Grant for Special Equipment from the Ministry of Education, Science and Culture, Japan.

References

(1) J.W. Menter, *Proc. Roy. Soc. London,* **A236**, 119 (1956).
(2) N. Uyeda, T. Kobayashi, K. Ishizuka and Y. Fujiyoshi, *Chem. Scripta,* **14**, 47 (1979).
(3) G. Binnig, H. Rohrer, Ch. Gerber and W. Weibel, *Phys. Rev. Lett.,* **50**, 120 (1983).
(4) S. Isoda, S. Moriguchi, H. Kurata, T. Kobayashi and N. Uyeda, *Ultramicroscopy,* **39**, 247 (1991).
(5) T. Kobayashi, S. Moriguchi, H. Kurata, T. Ogawa and S. Isoda, *Bull. Inst. Chem. Res., Kyoto Univ.,* **70**, 451 (1993).
(6) "High Resolution Transmission Electron Microscopy and Associated Techniques", ed. by P.R. Buseck, J.M. Cowley and L. Eyring, Oxford Univ. Press (1988).
(7) R.F. Egerton, "Electron Energy-Loss Spectroscopy in the Electron Microscope", Plenum Press (1989).
(8) H. Boersch, *Z. Phys.,* **139**, 115 (1954).
(9) Y. Ishida, H. Ichinose, M. Mori and M. Hashimoto, *Trans. Jpn. Inst. Met.,* **24**, 349 (1983).
W.M. Stobbs, G.J. Wood and D.J. Smith, *Ultramicroscopy,* **14**, 145 (1984).
G.J. Wood, W.M. Stobbs and D.J. Smith, *Phil. Mag.,* **A50**, 375 (1984).
(10) for example, R.W. Glaisher and A.E.C. Spargo, *Ultramicroscopy,* **18**, 323 (1985).
(11) Y. Fujiyoshi, T. Kobayashi, N. Uyeda, Y. Ishida and Y. Harada, *Ultramicroscopy,* **5**, 459 (1980).
(12) T. Kobayashi and N. Uyeda, *J. Cryst. Growth,* **84**, 589 (1987).
(13) C.W. Dirk, T. Inabe, K.F. Schoch and T.J. Marks, *J. Am. Chem. Soc.,* **105**, 1539 (1983).
(14) J.L. Hoard, G.H. Cohen and M.D. Glick, *J. Am. Chem. Soc.,* **89**, 1992 (1067).
(15) S. Isoda, I. Kubo, A. Hoshino, N. Asaka, H. Kurata and T. Kobayashi, *J. Cryst. Growth,* **115**, 388 (1991).
(16) S. Isoda, I. Kubo, A. Hoshino and T. Kobayashi, *Mol. Cryst. & Liq. Cryst.,* **218**, 195 (1992).
(17) Z.G. Li and P.J. Fagan, *Chem. Phys. Lett.,* **194**, 461 (1992).
(18) for example, R. Taylor, J.P. Hare, A.K. Abdul-Sada and H.W. Kroto, *J. Chem. Soc., Chem. Comm.,* **1990**, 1423 (1992).
(19) P.A. Heiney, J.E. Fischer, A.R. McGhie, W.J. Romanow, A.M. Denestein, J.P. McCauley, A.B. Smith and D.E. Cox, *Phys. Rev. Lett.,* **66**, 2911 (1991).
(20) K. Kikuchi, S. Suzuki, K. Saito, H. Shiromaru, I. Ikemoto, Y. Achiba, A.A. Zakihidov, A. Uga-

wa, K. Imaeda, H. Inokuchi and K. Yakushi, *Phys. C,* **185-189**, 415 (1991).
(21) S. Isoda, K. Saitoh, S. Moriguchi and T. Kobayashi, *Ultramicroscopy,* **35**, 329 (1991).
S. Isoda, K. Saitoh, T. Ogawa, S. Moriguchi and T. Kobayashi, *Ultramicroscopy,* **41**, 99 (1992).
(22) D.C. Dorset, W.F. Tival and J.N. Turner, *Acta Cryst.,* **A48**, 562 (1992).
(23) T. Ogawa, S. Moriguchi, S. Isoda and T. Kobayashi, *Proc. Ann. Meet. Cryst. Japan,* p.68 (1991).
T. Ogawa, S. Moriguchi, S. Isoda and T. Kobayashi, *Polymer Reprints, Japan,* **42**, 1337 (1992).